# Direct-Gap Semiconducting Tri-layer Silicene With 29% Photovoltaic Efficiency

Jian Lv,[&,†,#] Meiling Xu,[&,†] Shiru Lin, [§] Xuecheng Shao,[†] Xinyu Zhang,[†] Yanhui Liu,[‡] Yanchao Wang,[*,†] Zhongfang Chen,[§,*] Yanming Ma[†, ∞]

[†]State Key Lab of Superhard Materials, College of Physics, [#]College of Materials Science and Engineering and Key Laboratory of Automobile Materials of MOE, and [∞]International Center of Future Science, Jilin University, Changchun 130012, China

[‡]Department of Physics, College of Science, Yanbian University, Yanji 133002, China

[§] Department of Chemistry, University of Puerto Rico, Rio Piedras Campus, San Juan, PR 00931, USA

[&] The two authors contributed equally to this work and should be considered co-first authors

Corresponding Authors:

E-mail: wyc@calypso.cn (YW); zhongfangchen@gmail.com (ZC)

## Abstract

Crystalline silicon is dominating the current solar cell market due to the significant efficiency improvement and cost reduction in last decades. However, its indirect band gap nature leads to inefficient visible-light absorption, which seriously impedes further performance enhancement in silicon-based photovoltaic devices. Thus, it is highly desirable to develop direct band gap silicon materials. Herein, by means of ab initio swarm-intelligence structure-searching method, we predicted a quasi-direct gap semiconducting tri-layer silicene structure consisting of alternating arrays of six-membered Si rings, which can be converted into a direct gap semiconductor of 0.86 eV by applying a low tensile strain (~2.5%). Our calculations revealed that the photovoltaic efficiency of the tri-layer silicene reaches 29% at 1.0 μm, which is comparable to that of bulk GaAs with the highest conversion efficiency among thin-film solar cell absorbers.

**Keywords:** multi-layer silicene; photovoltaic materials; direct band gap; thin-flim solar cell

## INTRODUCTION

Recent years have witnessed a spectacular explosion of solar cells[1,2]. Most of the commercial solar cells are using crystalline silicon (c-Si) as the absorber layer[3–5] because of its elemental abundance, relatively low costs, ability for doping by other elements, and native oxide passivation layer. However, its indirect band gap nature[6] is the bottle neck for further improvement of the solar conversion efficiency. Consequently, several approaches have been developed to realize direct band gaps in c-Si[7–10], such as introducing various types of defects, engineering the electronic band structure through nanopatterning, applying strain, and designing metastable silicon crystal structures[11–20]. Despite their wide-ranging successes, these methods have some intrinsic limitations, for example, the defects can induce charge carrier traps or recombination centers, and metastable phase of silicon is difficult to be synthesized[21] because of relatively high energies.

Within the past few years, silicene has attracted tremendous attention due to their novel properties. Both monolayer and multilayer silicenes have been successfully grown on various metal substrates[22–29], especially on Ag (111). Depending on growth temperature and dynamics, various configurations have been observed, such as 3×3, $\sqrt{3}\times\sqrt{3}$ and $2\sqrt{3}\times2\sqrt{3}$ surface reconstructions with respect to the Si (111)-1×1 lattice[30–38], and some of them have been proved to exhibit moderate stability in air[39,40], thus holds a great promise for advanced applications on nanoscale electronics, photonics and spintronics, as well as for fundamental exploration of quantum properties.[41] Unfortunately, the silicene on metal substrate generally exhibits metallic or semi-metallic character without a bandgap[42], thus can not be used as adsorption layer of photovoltaic materials. Actually, substrate deeply impacts the optical absorbance of the multilayer silicene and consequently its photovoltaic efficiency.[43] Carrier

dynamics at the silicene/substrate interface indicate that the ultra-fast response is quite important in determining the appropriateness of a materials for photovoltaic applications.

Previous studies suggest that a significant band gap can be induced in thicker graphene samples[44,45]. Recent theoretical study of the multilayer silicene seems to support this conception[46]. Particularly, bilayer silicene sandwiched between planar crystals of $CaF_2$ and/or $CaSi_2$ has been successfully synthesized and exhibits semiconducting character[47]. Thus, the increase of layer thickness is an effective strategy to tune the band gap, further opens a door to design silicon-based photovoltaic materials with a suitable direct band gap.

Herein, we systemically investigated the low-lying energy structures of freestanding silicene phases from monolayer to penta-layer by means of *ab initio* swarm-intelligence structure-searching method. Density functional theory (DFT) calculations demonstrated that the electronic properties of multilayer silicene are extremely dependent on the number of layers. Notably, the lowest-energy tri-layer silicene (denoted as hex-*P*2/c-2×2) we predicted is energetically more favorable than previous reported $P2_1/m$-2×1 structure[46], and is semiconducting with a quasi-direct band gap. The indirect-direct band gap transition can occur upon a small external strain in the hex-*P*2/c-2×2 trilayer silicene, and its estimated photovoltaic efficiency (29%) is comparable to that of bulk GaAs, which has the highest conversion efficiency among thin-film solar cell absorbers. Therefore, the hex-*P*2/c-2×2 phase holds great potential as ideal candidates for high-efficiency photovoltaic absorbers.

## COMPUTATIONAL METHOD

The low-energy structures of silicene films were searched by the swarm-intelligence CALYPSO method[48–51], which has been benchmarked on various systems, ranging from elemental to binary and ternary compounds[52–57]. In general, the simulation cells contain up to

64 atoms, the population size is set to 40, and the structure search is terminated after generating 2,000 structures for each run. Geometric optimizations, electronic structure and phonon dispersion computations were performed in the density functional theory (DFT) framework within the generalized gradient approximation (GGA), as implemented in the VASP code.[58] The van der Waals density functional, namely optB86b-vdW[59,60], was adopted to treat dispersion forces. A vacuum region of ~20 Å was applied for multilayer silicenes with and without silver substrate, and Monkhorst-Pack *k* meshes were chosen for Brillouin zone sampling to ensure that all the energy calculations are well converged to ~ 1meV. The Heyd−Scuseria−Ernzerhof (HSE) hybrid functional[61] and the GLLB-sc functional[62–64] were employed to evaluate the electronic band structures. The dynamic stability of the predicted structures was verified by phonon dispersion analyses through the direct supercell method, as implemented in the PHONOPY code[65,66].

## RESULTS AND DISCUSSION

We have performed extensive structural searches for the most stable phases of silicene from the monolayer to penta-layer *via* swarm-intelligence CALYPSO method. Our search successfully identified the experimentally available (w-BLSi bilayer[47]) or theoretically predicted (eg. *Cmme*-1×1[67] and hex-OR-2×2 bilayers[68], $P2_1/m$-2×1 tri- or quad-layers[46] structures (Figure S1), validating our structure-searching methodology for applications with multi-layer silicene structures.

**Geometrical Structures, Stabilities, and Electronic Properties of Tri-layer Silicene.** Due to the complexity of the tri-layer silicene arrangement, diverse structures with various stacking and periodicity features are energetically competitive. Fig. 1 depicts the low-lying

energy tri-layer silicene structures, while Table 1 lists their structural features together with the energetic data. Clearly, the predicted structures fall into three groups according to their energies and general structural features.

The first group has two members: the lowest-energy tri-layer silicene with *P*2/*c* symmetry resembles reconstructed hexagonal-phase (hex) Si (1-10) surface, thus is denoted as hex-*P*2/c-2×2; and the other structure of trilayer with *Pm* space group (denoted as hex-*Pm*-2×1) is predicted to be less favourable than hex-*P2/c*-2×2 by only ~5 meV/atom. The hex-*P2/c*-2×2 trilayer consists of alternating arrays of six-membered Si rings, and the protruding Si atoms with threefold coordination form a staggered Si-dimer pattern; the hex-*Pm*-2×1 trilayer also contains six-membered Si rings, while the protruding Si atoms form a parallel Si-dimer configures.

The $P2_1/m$-2×1[46] trilayer characterized by Si(111)-2×1 surface reconstruction is the only member in the second group, consists of reconstructed five- and seven-membered Si rings, and is energetically less favorable than hex-*P2/c*-2×2 by 41.6 meV/atom. As the sole member of the third group, the *Pm*-2×1 tri-layer is 67.7 meV/atom higher in energy than hex-*P2/c*-2×2, and its top and bottom silicene layers are drastically reconstructed to form four- and eight-membered rings.

The hex-*P*2/c-2×2 and hex-*Pm*-2×1 in the first group are not only most favorable among tri-layer silicenes discussed above, but also lower in energy than those proposed before. For example, the current hex-*P*2/c-2×2 is 95.0 meV and 41.6 meV/atom lower in energy than the structures with non-reconstructed ABC stacking configuration[69,35](Figure S2) and Si(111)-2×1 surface reconstruction (the aforementioned $P2_1/m$-2×1)[45], respectively. Previous theoretical studies[70] proposed layered dumbbell silicene structures (LDS) based on

structural transformations in grown layers on Ag (111), but the tri-layer eclipsed LDS and staggered LDS structures are 58.9 meV and 53.3 meV/atom higher in energy, respectively, than the current hex-*P*2/c-2×2. We also constructed the 5 × 5 and 7 × 7 tri-layer silicene phases, whose initial surface structures are the same as the Si(111)-5×5 and 7×7 surfaces with the dimer adatom-stacking fault models (DAS). Our geometry optimizations of these Si(111)-5×5 and 7×7 DAS phases led to the distorted unphysical structures, indicating that the Si(111)-5×5 and 7×7 DAS structures are unstable for tri-layer silicene. Our results are consistent with previous reports[45].

The high thermodynamic stability of tri-layer silicenes in the first group may be rationalized by the larger proportion of $sp^3$-hybrized fourfold-coordinated Si (75.0% for hex-*P*2/c-2×2 and 66.7% for hex-*Pm*-2×1) than other competing structures (Table 1). Moreover, these two structures were confirmed to be dynamically stable, as evidenced by the absence of imaginary phonon modes in the whole Brillouin zone [Figure S3].

Note that both monolayer and multi-layer silicenes were synthesized on substrates, especially on Ag(111), using molecular beam epitaxy. To further assess the experimental accessibility of hex-*P*2/c-2×2, the lowest-energy tri-layer silicene, we optimized its structure on Ag(111) substrate and computed its cohesive ($E_c$) and binding energies ($E_b$) (see Supporting Information for the definition of cohesive and binding energies, as well as the computational details. Basically, more positive $E_c$ and $E_b$ values indicate higher thermodynamic stability and stronger interactions between silicene layer and the substrate). The 2×2 supercell of hex-P2/c-2×2 on a five-layered 5×5 Ag (111) slab was chosen in our computations (Figure S4a). After full structure relaxation, the bottom layer of hex-*P*2/c-2×2 adopts the bulk Si(111) structure due to the strong Ag-Si interactions, while the top layer

maintains the hex-P2/c-2×2 configuration. Strikingly, the cohesive energy ($E_c$) of hex-P2/c-2×2 on Ag(111) substrate is 10.0 meV/atom higher than that of the experimentally realized tri-layer silicene[35] which adopts ABC-stacking configuration of Si(111) with a $\sqrt{3}\times\sqrt{3}$ termination (Figure S4b). The binding energy ($E_b$) of hex-P2/c-2×2 is 100.0 meV/atom lower that of the experimental tri-layer silicene, suggesting that the hex-P2/c-2×2 can be relatively easier to remove from the substrate once synthesized. These results indicate that a superior thermodynamic stability and high experimental accessibility of the hex-P2/c-2×2 on Ag(111) substrate. Below, we will focus on the properties of hex-*P*2/c-2×2 and hex-*Pm*-2×1 trilayers in the first group.

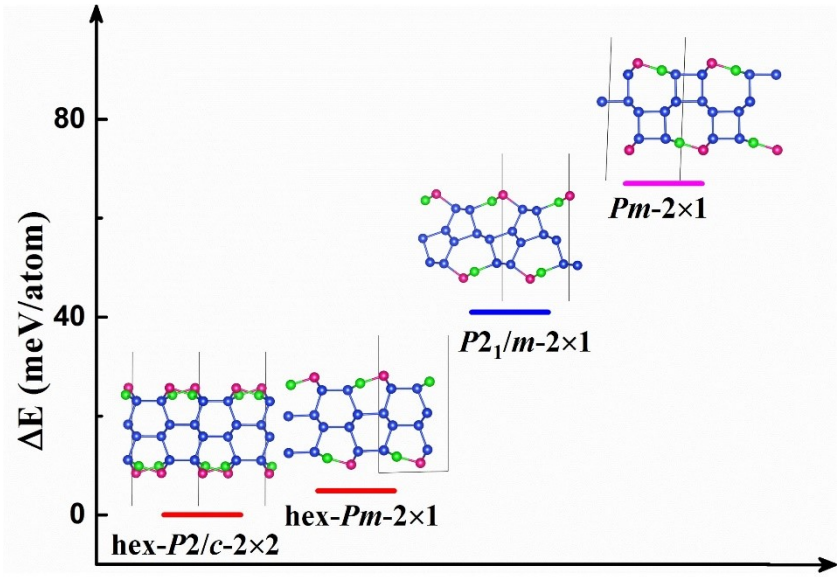


FIG. 1. Side views of the lowest-energy and low-lying structures of freestanding tri-layer silicene. The highly protruded Si atoms at the surfaces, the second-most protruded Si atoms, and the remaining ones are depicted by magenta, green and blue balls, respectively. The unit cells are indicated by solid lines. The energies are relative to the most stable hex-*P*2/c-2×2 structure.

**Table 1.** Structural features, relative energies (ΔE, meV/atom), proportion of $sp^3$-hybridized fourfold-coordinated Si ($sp^3$ Si %), and band gap ($E_g$, eV, at HSE06) and the

nature of the band gaps of the tri-layer silicene structures. QD and ID stand for quasi-direct band gap and indirect band gap, respectively.

| | | $\Delta E_{PBE}$ | $sp^3$ Si % | $E_g$ | Type |
|---|---|---|---|---|---|
| hex-P2/c-2×2 | Six-membered rings | 0.0 | 75.0 | 0.76 | QD |
| hex-Pm-2×1 | | 5.0 | 66.7 | 0.79 | ID |
| $P2_1$/m-2×1 | Five and seven-membered rings | 41.6 | 66.7 | 0.48 | ID |
| Pm-2×1 | Four and eight-membered rings | 67.7 | 66.7 | 0.63 | ID |

We calculated the band structures and projected density of states (PDOS) of the two isoenergetic tri-layer phases, hex-*P*2/*c*-2×2 and hex-*Pm*-2×1, using the HSE06 functional. The hex-*P*2/c-2×2 phase is semiconducting with a quasi-direct band gap of 0.76 eV (Fig. 2a). The global VBM is located at the zone-center Γ point, while the overall CBM is located at (-0.2 0.2 0) but is only 0.06 eV lower than the CBM at the Γ point. In comparison, the hex-*Pm*-2×1 phase is semiconducting with an indirect band gap of 0.79 eV (Fig. 2b). The partial charge densities of the VBM and CBM of these two phases (Fig. 2) have similar features: the charge density of the VBM is mainly contributed by the hybridization of the π ($p_z$) and σ orbitals of the three-folded surface Si atoms, while most of the charge density of the CBM originates from the π orbitals of three-folded Si atoms. The band structures of hex-*P*2/*c*-2×2 and hex-*Pm*-2×1 are in sharp contrast to various stacking configurations of Si(111), all of which exhibit metallic or semi-metallic character without a band gap (see Figure S2, for more details on how the stacking pattern determines the structural and electronic properties, please refer to Ref. 68).

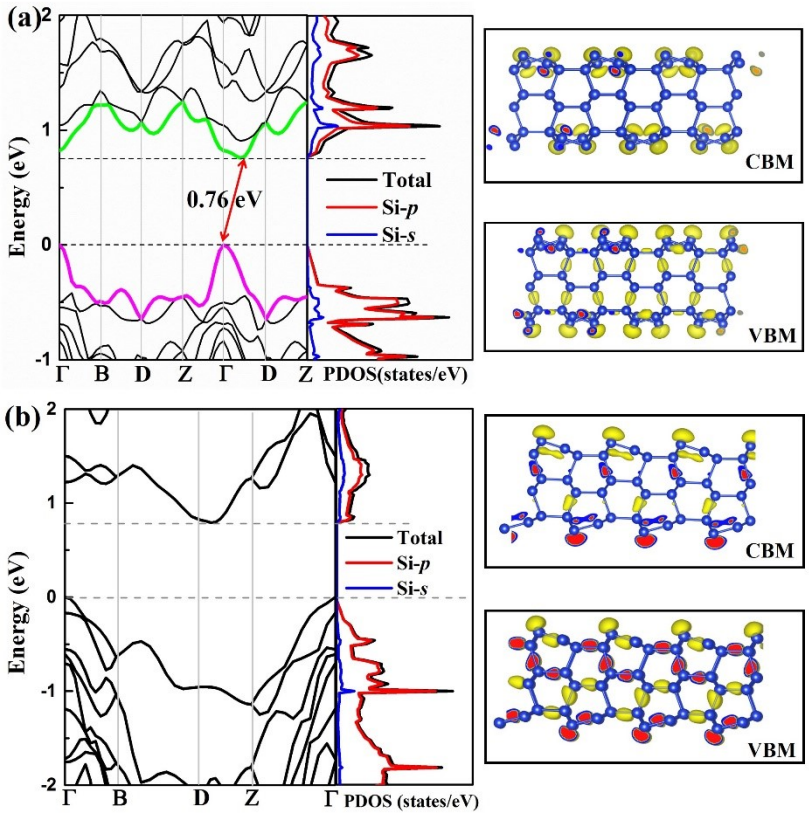


FIG. 2. The calculated band structures and projected density of states (PDOS) for (a) hex-*P*2/*c*-2×2 structure and (b) hex-*Pm*-2×1 at HSE06 level. The partial charge densities of the VBM and CBM are also plotted. The Fermi level is set to zero.

**Strain-Induced Band-Gap Engineering of hex-*P*2/*c*-2×2 Silicene and Its Potential Application in High-Performance Solar Cells.** Strain is an effective approach to tune band gaps[71,72], and low strain easily occurs for 2D materials during their growth on different substrates through lattice mismatch. Therefore, we applied a biaxial strain, as depicted in Fig. 3a, on the hex-*P*2/*c*-2×2 tri-layer silicene to investigate the resultant electronic properties. Our calculations showed that the band gap of hex-*P*2/*c*-2×2 phase can be engineered by applying a biaxial strain, and the 2.5% tensile strain leads to the maximum band gap of 0.86

eV (Fig. 3b and c). Interestingly, at this tensile strain, both the VBM and CBM are located at the Γ point, leading to a direct semiconductor.

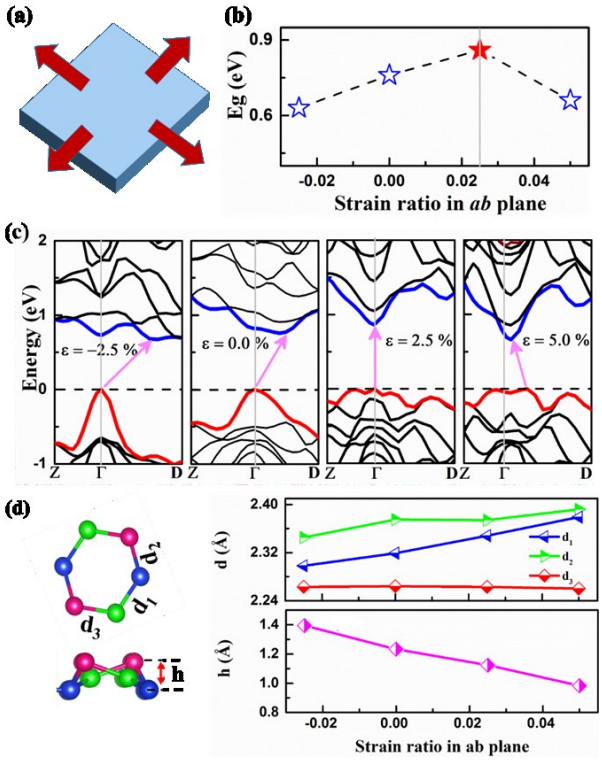


FIG. 3. (a) Schematic representation of the hex-*P*2/c-2×2 phase of tri-layer silicene under biaxial tensile strain. (b) Plots of the energy band gap versus the applied biaxial compressive and tensile strain for the hex-*P*2/c-2×2 phase. (c) Electronic band structures of the hex-*P*2/c-2×2 phase under -2.5%, 0.0%, 2.5%, and 5.0% strain found using the HSE06 functional. (d) Calculated structural parameters as a function of the biaxial compressive and tensile strain.

To further investigate the strain effect to the electronic properties of hex-*P*2/c-2×2, we examined the detailed variation of the band structures as a function of applied strains (Fig. 3c). Though both sensitive to strains, the valence and conduction bands response differently upon external strains: under tensile strain, the conduction bands become more dispersive as evidenced by the enlarged band width, while the valence bands tend to less dispersive; under compressive strain, conduction bands narrow while valence bands widen with increasing strains.

The band structure variation is the consequence of the structural parameter change under external strains (Fig. 3d). The Si-Si dimer bond length ($d_3$) is almost unchanged under tensile or compressive strain. However, with increasing the tensile strain, other Si-Si bond lengths ($d_1$ and $d_2$) in the Si six-membered rings increase, and the six-membered rings become flattened, as revealed by the decreasing surface layer thickness (h). Such a flattening enhances the $sp^2$ hybridization in six-membered Si rings. As aforementioned, the CBM is primarily composed of the π ($p_z$) orbitals of the three-folded Si atoms on the surface, while the VBM originates from both the π ($p_z$) orbitals of the three-folded Si atoms on the surface and the σ orbitals of the inner four-folded Si atoms (Fig. 3b). Clearly, the enhancement of the $sp^2$ hybridization in six-membered Si rings induces more delocalized π ($p_z$) orbitals and localized σ orbitals, which leads to more dispersive conduction bands but less dispersive valence bands.

The direct band-gap (0.86 eV) semiconducting nature endows the hex-*P*2/c-2×2 tri-layer silicene under 2.5% tensile strain promising applications in photovoltaics. Thus, we estimated the theoretical maximum solar cell efficiency of hex-*P*2/c-2×2 phase by calculating its spectroscopic limited maximum efficiency (SLME) based on the improved Shockley-Queisser model[73], which captures the band gap size, the band gap type (direct versus indirect), the absorption spectrum and material-dependent non-radiative recombination loss. The simulation was performed under the standard AM1.5G solar spectrum at room temperature.

As indicated in Fig. 4, the optical absorption coefficient of hex-*P*2/c-2×2 tri-layer silicene reaches $\sim 10^4$–$10^5$ $cm^{-1}$, which is at the same order of magnitude as that of GaAs. Thus, the

photovoltaic efficiencies of the hex-*P*2/c-2×2 structure is comparable to that of the widely used GaAs thin-film solar absorbers, and far beyond that of c-Si. Particularly, at a film thickness of ~1 μm, hex-*P*2/c-2×2 silicene achieves a conversion efficiency of 29%, which is only slightly lower than that of GaAs (32%), which has the highest conversion efficiency among thin-film solar cell absorbers. Note that the 1 μm thickness of tri-layer hex-*P*2/c-2×2 silicene could be experimentally engineered by van de Waals stacking.

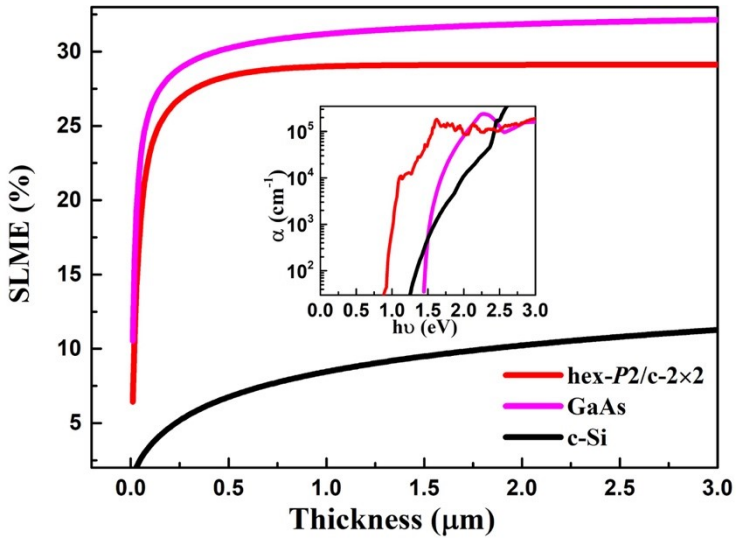


FIG. 4. The theoretical photovoltaic efficiency as a function of slab thickness for hex-*P*2/c-2×2 compared with bulk Si and GaAs. The inset shows their adsorption spectra.

**Geometric Structures and Electronic Properties of Multilayer Silicene with Different Number of Layers.** To gain a better understanding of structural evolution of multilayer silicene, we also performed structural searches for the thicker silicenes, *i.e.*, the quad-layer and penta-layer (Fig. 5a). Our computations revealed that the quad-layer and penta-layer both consist of alternating arrays of six-membered Si rings in the ground state, exhibiting similar features as the tri-layer silicene. Based on these structural features, we further constructed the multi-layer silicenes with six and seven layers. Fig. 5a summarizes the total energies (in meV/atom) of hex-*P*2/c-2×2 silicenes with three to seven layers with

respect to the previously reported tri-layer $P2_1/m$-2×1 (Si (111)-2×1) silicene[46], the energies for quad-layer silicenes with Si(111)-5×5 and 7×7 DAS surface reconstructions are also given for comparison. Interestingly, our predicted structural model with quad-layer is lower in energy than Si(111)-5×5 and 7×7 DAS models by 58.0 meV/atom and 35.3 meV/atom, respectively (Fig. 5a).

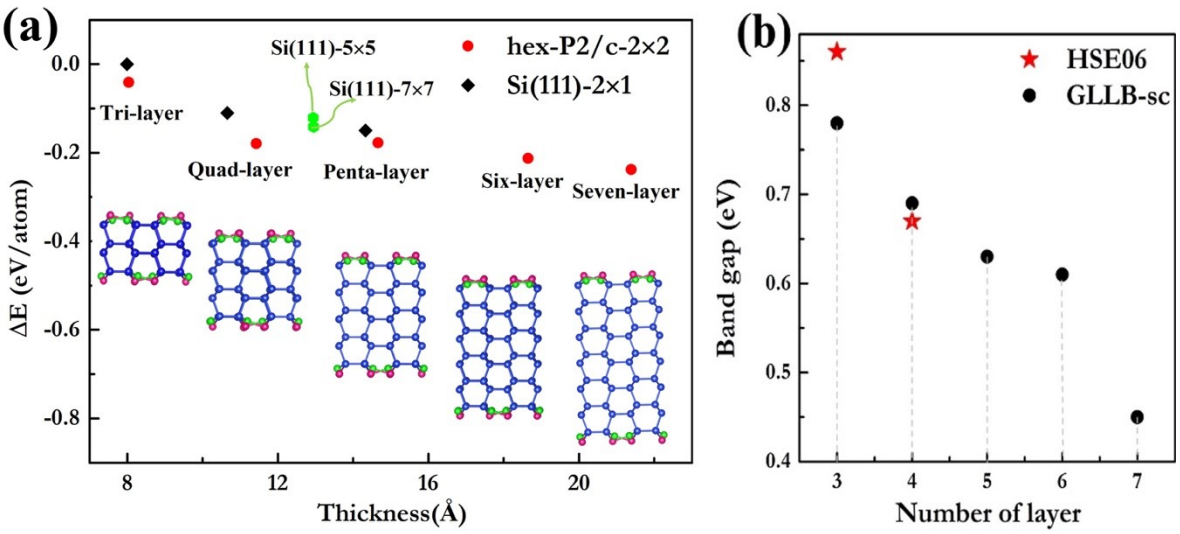


FIG. 5. (a) The total energies (in eV/atom) of hex-$P2$/c-2×2 silicenes with three to seven layers with respect to the previously reported tri-layer $P2_1/m$-2×1 (Si (111)-2×1) silicene[46], the energies for quad-silicenes with Si(111)-5×5 and 7×7 DAS surface reconstructions are given for comparison. (b) The band gaps of the lowest-energy phases of silicenes from tri-layer to seven-layer computed using the GLLB-sc functional, in comparison with the results by HSE06 functional.

Then, we examined the electronic structure evolution with increase layer numbers in the multi-layer silicenes using the GLLB-sc (Figure 5b) and PBE functionals (Figure S6), respectively. According to our calculations, the band gap of hex-P2/c-2×2-type structures decreases with increasing number of stacking layers, the tri-layer hex-P2/c-2×2 structure has the largest band gap (0.76 eV), which is still smaller than that of c-Si (1.12 eV). Thus, it is reasonable to expect that the multi-layer silicene will have a minimum band gap at a certain

number of stacking layers, beyond which the band gap will gradually increase and eventually transform to that of c-Si. Our calculations showed that the transition would occur beyond 10-layers, since the band gap continues to decrease to 0.09 eV at this thickness [Figure S7].

Recent experimental work by Grazianetti *et al.* found that the multi-layer silicene without Ag exhibits ambipolar transport behavior in field-effect transistor device[74]. Motivated by this observation, we calculated the DOS of 10-layer hex-P2/c-2×2 silicene, whose thickness is the same as the experimentally fabricated multi-layer silicene. Strikingly, the very small band gap of 0.09 eV for the 10-layer hex-P2/c-2×2 silicence is consistent with experimental results[74].

Interestingly, the odd-even layers can alter intrinsic band gaps, i.e. odd-layers exhibit quasi-direct characteristics, in contrast, even-layer ones possess indirect characteristics (Figure S6). To understand this trend, we carefully analyzed the band structures of the tri-layer and quad-layer silicenes at HSE functional level, which serve as representatives for odd- and even-layer silicenes. In Figure S8, for both tri-layer and quad-layer silicenes, the global valence band maximum (VBM) is located at the zone-center Γ point. However, the situation for CBM is different: the overall conduction band maximum (CBM) is located at (-0.2 0.2 0) (only 0.06 eV higher than the CBM at the Γ point) for tri-layer silicene, leading to its quasi-direct band gap; while the CBM is at M point (0.5 0 0) for quad-layer (0.16 eV higher than the CBM at the Γ point), leading to its indirect band gap nature. This difference can be explained in terms of the symmetry of the crystal space group and mass density. For a tri-layer with *P*2/c symmetry, its mass density is 0.76 g/cm$^3$. In comparison, a quad-layer with *C*2/m symmetry has a smaller mass density of 0.51 g/cm$^3$, leading to its in-plane lattice compression and stretched out-of-plane component of Si-Si bonds. Upon increasing in-plane

compressive strain due to the Possion effect, the CBM composed of Si $p_z$ orbitals at the M point for quad-layer shifts to lower energies with respect to the CBM of tri-layer.

Since PBE tends to underestimate band gap values, we adopt the GLLB-sc functional[62–64] to get more accurate band gaps for the multi-layer silicenes. Our test computations showed that GLLB-sc gave comparable band gap values to those obtained by HSE06 functional for tri- and quad-layer silicenes (Fig. 5b), which validate its suitability to estimate the band gaps of the systems under study. We found that the band gaps decrease from 0.78 eV to 0.45 eV when increasing the layer number from three to seven, thus the band gap value and the band gap nature (indirect or quasi-direct) can be tuned by controlling the layer numbers.

In conclusion, we systematically studied the low-laying phases of silicene from the monolayer to hept-layer by employing a swarm-intelligence algorithm and *ab initio* calculations. We found that controlling the layer thickness is an effective strategy to tune the band gap. More important, the energetically most stable tri-layer hex-*P*2/c-2×2 structure is a quasi-direct semiconductor, and can be converted into a direct gap semiconductor of 0.86 eV (at HSE) by applying a low tensile strain (~2.5%), which possesses a high photovoltaic efficiency of up to 29%. This study not only identified promising materials for flexible and wearable photovoltaic devices, but also provides a general method to study the geometric structure and electronic property evolution for 2D materials with nonlayered bulk counterparts.

Associated Content

**Supporting Information**. Structures and total energies of freestanding other low-lying tri-layer silicene not shown in text, phonon dispersions for hex-*P*2/c-2×2 and hex-*Pm*-2×1 structures; calculated band structures of other low-lying tri-layer silicene not shown in text

using the HSE06 functional; crystallographic data for hex-*P*2/c-2×2, hex-*Pm*-2×1, $P2_1$/m-2×1, and *P*m-2×1 phases.

**ACKNOWLEDGMENT**

The authors acknowledge funding support from the National Natural Science Foundation of China under Grants No. 11774127, No. 11534003 and No. 11764043; the National Key Research and Development Program of China under Grant No. 2016YFB0201200, No. 2016YFB0201201, and No. 2017YFB0701503; the 2012 Changjiang Scholars Program of China supported by Program for JLU Science and Technology Innovative Research Team (JLUSTIRT); the Science Challenge Project, No. TZ2016001 and the NSF-CREST Center for Innovation, Research and Education in Environmental Nanotechnology (CIRE2N) (Grant Number HRD-1736093) and NASA (Grant 17-EPSCoRProp-0032). Part of the calculation was performed in the high performance computing center of Jilin University and at Tianhe2-JK in the Beijing Computational Science Research Center.

**References**


(1) Petter Jelle, B.; Breivik, C.; Drolsum Røkenes, H. *Sol. Energy Mater. Sol. Cells* **2012**, *100* (7465), 69–96.
(2) Green, M. A. *Sol. Energy* **2003**, *74* (3), 181–192.
(3) Hao, L.; Liu, Y.; Gao, W.; Han, Z.; Xue, Q.; Zeng, H.; Wu, Z.; Zhu, J.; Zhang, W. *J. Appl. Phys.* **2015**, *117* (11), 114502.
(4) Nagamatsu, K. A.; Avasthi, S.; Jhaveri, J.; Sturm, J. C. *IEEE J. Photovoltaics* **2014**, *4* (1), 260–264.
(5) Kim, D. Y.; Santbergen, R.; Tan, H.; van Swaaij, R. A. C. M. M.; Smets, A. H. M.; Isabella, O.; Zeman, M. *Appl. Phys. Lett.* **2014**, *105* (6), 63902.
(6) Hybertsen, M. S.; Louie, S. G. *Phys. Rev. Lett.* **1985**, *55* (13), 1418–1421.
(7) Moontragoon, P.; Ikonić, Z.; Harrison, P. *Semicond. Sci. Technol.* **2007**, *22* (7), 742–748.
(8) Bo, X. Z.; Rokhinson, L. P.; Yin, H.; Tsui, D. C.; Sturm, J. C. *Appl. Phys. Lett.* **2002**, *81* (17), 3263–3265.
(9) Hong, K. H.; Kim, J.; Lee, S. H.; Shin, J. K. *Nano Lett.* **2008**, *8* (5), 1335–1340.
(10) Oh, Y. J.; Lee, I.-H.; Kim, S.; Lee, J.; Chang, K. J. *Sci. Rep.* **2016**, *5* (1), 18086.
(11) Xiang, H. J.; Huang, B.; Kan, E.; Wei, S.-H.; Gong, X. G. *Phys. Rev. Lett.* **2013**, *110* (11), 118702.
(12) Fan, Q.; Chai, C.; Wei, Q.; Yan, H.; Zhao, Y.; Yang, Y.; Yu, X.; Liu, Y.; Xing, M.; Zhang, J.; Yao, R. *J. Appl. Phys.* **2015**, *118* (18), 185704.
(13) Fan, Q.; Chai, C.; Wei, Q.; Yang, Y. *Phys. Chem. Chem. Phys.* **2016**, *18* (18), 12905–12913.
(14) He, C.; Zhang, C.; Li, J.; Peng, X.; Meng, L.; Tang, C.; Zhong, J. *Phys. Chem. Chem. Phys.* **2016**, *18* (14), 9682–9686.
(15) Kim, D. Y.; Stefanoski, S.; Kurakevych, O. O.; Strobel, T. A. *Nat. Mater.* **2014**, *14* (2), 169–173.
(16) Lee, I.-H.; Lee, J.; Oh, Y. J.; Kim, S.; Chang, K. J. *Phys. Rev. B* **2014**, *90* (11), 115209.
(17) Mujica, A.; Pickard, C. J.; Needs, R. J. *Phys. Rev. B* **2015**, *91* (21), 214104.
(18) Amsler, M.; Botti, S.; Marques, M. A. L.; Lenosky, T. J.; Goedecker, S. *Phys. Rev. B* **2015**, *92* (1), 014101.
(19) Guo, Y.; Wang, Q.; Kawazoe, Y.; Jena, P. *Sci. Rep.* **2015**, *5* (1), 14342.
(20) Wang, Q.; Xu, B.; Sun, J.; Liu, H.; Zhao, Z.; Yu, D.; Fan, C.; He, J. *J. Am. Chem. Soc.* **2014**, *136* (28), 9826–9829.
(21) Botti, S.; Flores-Livas, J. A.; Amsler, M.; Goedecker, S.; Marques, M. A. L. *Phys. Rev. B - Condens. Matter Mater. Phys.* **2012**, *86* (12), 31–33.
(22) Meng, L.; Wang, Y.; Zhang, L.; Du, S.; Wu, R.; Li, L.; Zhang, Y.; Li, G.; Zhou, H.; Hofer, W. A.; Gao, H. J. *Nano Lett.* **2013**, *13* (2), 685–690.
(23) Lalmi, B.; Oughaddou, H.; Enriquez, H.; Kara, A.; Vizzini, Ś.; Ealet, B.; Aufray, B. *Appl. Phys. Lett.* **2010**, *97* (22), 2008–2010.
(24) De Padova, P.; Vogt, P.; Resta, A.; Avila, J.; Razado-Colambo, I.; Quaresima, C.; Ottaviani, C.; Olivieri, B.; Bruhn, T.; Hirahara, T.; Shirai, T.; Hasegawa, S.; Carmen Asensio, M.; Le Lay, G. *Appl. Phys. Lett.* **2013**, *102* (16), 163106.
(25) Feng, B.; Ding, Z.; Meng, S.; Yao, Y.; He, X.; Cheng, P.; Chen, L.; Wu, K. *Nano Lett.* **2012**, *12* (7), 3507–3511.
(26) Fleurence, A.; Friedlein, R.; Ozaki, T.; Kawai, H.; Wang, Y.; Yamada-Takamura, Y. *Phys. Rev. Lett.* **2012**, *108* (24), 245501.

(27) Aufray, B.; Kara, A.; Vizzini, S.; Oughaddou, H.; Léandri, C.; Ealet, B.; Le Lay, G. *Appl. Phys. Lett.* **2010**, *96* (18), 183102.
(28) Limit, D. *ACSNano* **2014**, *8* (7), 7538.
(29) De Padova, P.; Avila, J.; Resta, A.; Razado-Colambo, I.; Quaresima, C.; Ottaviani, C.; Olivieri, B.; Bruhn, T.; Vogt, P.; Asensio, M. C.; Le Lay, G. *J. Phys. Condens. Matter* **2013**, *25* (38), 382202.
(30) Feng, B.; Li, H.; Liu, C.-C.; Shao, T.-N.; Cheng, P.; Yao, Y.; Meng, S.; Chen, L.; Wu, K. *ACS Nano* **2013**, *7* (10), 9049–9054.
(31) Chen, J.; Du, Y.; Li, Z.; Li, W.; Feng, B.; Qiu, J.; Cheng, P.; Xue Dou, S.; Chen, L.; Wu, K. *Sci. Rep.* **2015**, *5*(4), 13590.
(32) Chen, L.; Liu, C.-C.; Feng, B.; He, X.; Cheng, P.; Ding, Z.; Meng, S.; Yao, Y.; Wu, K. *Phys. Rev. Lett.* **2012**, *109* (5), 056804.
(33) Qiu, J.; Fu, H.; Xu, Y.; Oreshkin, A. I.; Shao, T.; Li, H.; Meng, S.; Chen, L.; Wu, K. *Phys. Rev. Lett.* **2015**, *114* (12), 126101.
(34) Chen, L.; Li, H.; Feng, B.; Ding, Z.; Qiu, J.; Cheng, P.; Wu, K.; Meng, S. *Phys. Rev. Lett.* **2013**, *110* (8), 085504.
(35) Fu, H.; Chen, L.; Chen, J.; Qiu, J.; Ding, Z.; Zhang, J.; Wu, K.; Li, H.; Meng, S. *Nanoscale* **2015**, *7* (38), 15880–15885.
(36) Fu, H.; Zhang, J.; Ding, Z.; Li, H.; Meng, S. *Appl. Phys. Lett.* **2014**, *104* (13), 131904.
(37) Chen, L.; Feng, B.; Wu, K. *Appl. Phys. Lett.* **2013**, *102* (8), 81602.
(38) Qiu, J.; Fu, H.; Xu, Y.; Zhou, Q.; Meng, S.; Li, H.; Chen, L.; Wu, K. *ACS Nano* **2015**, *9* (11), 11192–11199.
(39) De Padova, P.; Ottaviani, C.; Quaresima, C.; Olivieri, B.; Imperatori, P.; Salomon, E.; Angot, T.; Quagliano, L.; Romano, C.; Vona, A.; Muniz-Miranda, M.; Generosi, A.; Paci, B.; Lay, G. Le. *2D Mater.* **2014**, *1* (2), 021003.
(40) Li, H.; Hui-Xia, F.; Meng, S. *Chinese Phys. B* **2015**, *24* (8), 1–10.
(41) Molle, A.; Goldberger, J.; Houssa, M.; Xu, Y.; Zhang, S.-C.; Akinwande, D. *Nat. Mater.* **2017**, *16* (2), 163–169.
(42) Zhao, J.; Liu, H.; Yu, Z.; Quhe, R.; Zhou, S.; Wang, Y.; Liu, C. C.; Zhong, H.; Han, N.; Lu, J.; Yao, Y.; Wu, K. *Prog. Mater. Sci.* **2016**, *83*, 24–151.
(43) Cinquanta, E.; Fratesi, G.; Dal Conte, S.; Grazianetti, C.; Scotognella, F.; Stagira, S.; Vozzi, C.; Onida, G.; Molle, A. *Phys. Rev. B - Condens. Matter Mater. Phys.* **2015**, *92* (16), 165427.
(44) Lui, C. H.; Li, Z.; Mak, K. F.; Cappelluti, E.; Heinz, T. F. *Nat. Phys.* **2011**, *7* (12), 944–947.
(45) Bao, W.; Jing, L.; Velasco, J.; Lee, Y.; Liu, G.; Tran, D.; Standley, B.; Aykol, M.; Cronin, S. B.; Smirnov, D.; Koshino, M.; McCann, E.; Bockrath, M.; Lau, C. N. *Nat. Phys.* **2011**, *7* (12), 948–952.
(46) Guo, Z.-X.; Zhang, Y.-Y.; Xiang, H.; Gong, X.-G.; Oshiyama, A. *Phys. Rev. B* **2015**, *92* (20), 201413.
(47) Yaokawa, R.; Ohsuna, T.; Morishita, T.; Hayasaka, Y.; Spencer, M. J. S.; Nakano, H. *Nat. Commun.* **2016**, *7*, 10657.
(48) Wang, Y.; Lv, J.; Zhu, L.; Ma, Y. *Phys. Rev. B* **2010**, *82* (9), 094116.
(49) Wang, Y.; Lv, J.; Zhu, L.; Ma, Y. *Comput. Phys. Commun.* **2012**, *183* (10), 2063–2070.
(50) Wang, Y.; Lv, J.; Zhu, L.; Lu, S.; Yin, K.; Li, Q.; Wang, H.; Zhang, L.; Ma, Y. *J. Phys. Condens. Matter* **2015**, *27* (20), 203203.

(51) Wang, Y.; Miao, M.; Lv, J.; Zhu, L.; Yin, K.; Liu, H.; Ma, Y. *J. Chem. Phys.* **2012**, *137* (22), 224108.
(52) Xu, M.; Shao, S.; Gao, B.; Lv, J.; Li, Q.; Wang, Y.; Wang, H.; Zhang, L.; Ma, Y. *ACS Appl. Mater. Interfaces* **2017**, *9* (9), 7891–7896.
(53) Lv, J.; Wang, Y.; Zhu, L.; Ma, Y. *Phys. Rev. Lett.* **2011**, *106* (1), 015503.
(54) Zhu, L.; Liu, H.; Pickard, C. J.; Zou, G.; Ma, Y. *Nat. Chem.* **2014**, *6* (7), 644–648.
(55) Zhu, L.; Wang, H.; Wang, Y.; Lv, J.; Ma, Y.; Cui, Q.; Ma, Y.; Zou, G. *Phys. Rev. Lett.* **2011**, *106* (14), 145501.
(56) Wang, H.; Tse, J. S.; Tanaka, K.; Iitaka, T.; Ma, Y. *Proc. Natl. Acad. Sci.* **2012**, *109* (17), 6463–6466.
(57) Li, Y.; Hao, J.; Liu, H.; Li, Y.; Ma, Y. *J. Chem. Phys.* **2014**, *140* (17), 174712.
(58) Kresse, G.; Furthmüller, J. *Phys. Rev. B* **1996**, *54* (16), 11169–11186.
(59) Klime, J.; Bowler, D. R.; Michaelides, A. *Phys. Rev. B - Condens. Matter Mater. Phys.* **2011**, *83* (19), 195131.
(60) Dion, M.; Rydberg, H.; Schröder, E.; Langreth, D. C.; Lundqvist, B. I. *Phys. Rev. Lett.* **2004**, *92* (24), 246401.
(61) Heyd, J.; Scuseria, G. E.; Ernzerhof, M. *J. Chem. Phys.* **2003**, *118* (18), 8207–8215.
(62) Li, H.; Tsai, C.; Koh, A. L.; Cai, L.; Contryman, A. W.; Fragapane, A. H.; Zhao, J.; Han, H. S.; Manoharan, H. C.; Abild-Pedersen, F.; Nørskov, J. K.; Zheng, X. *Nat. Mater.* **2016**, *15* (1), 48–53.
(63) Miró, P.; Ghorbani-Asl, M.; Heine, T. *Angew. Chemie Int. Ed.* **2014**, *53* (11), 3015–3018.
(64) Castelli, I. E.; Olsen, T.; Datta, S.; Landis, D. D.; Dahl, S.; Thygesen, K. S.; Jacobsen, K. W. *Energy Environ. Sci.* **2012**, *5* (2), 5814–5819.
(65) Parlinski, K.; Li, Z.; Kawazoe, Y. *Phys. Rev. Lett.* **1997**, *78* (21), 4063–4066.
(66) Togo, A.; Oba, F.; Tanaka, I. *Phys. Rev. B* **2008**, *78* (13), 134106.
(67) Luo, W.; Ma, Y.; Gong, X.; Xiang, H. *J. Am. Chem. Soc.* **2014**, *136* (45), 15992–15997.
(68) Sakai, Y.; Oshiyama, A. *Phys. Rev. B* **2015**, *91* (20), 201405.
(69) Kamal, C.; Chakrabarti, A.; Banerjee, A.; Deb, S. K. *J. Phys. Condens. Matter* **2013**, *25* (8), 85508.
(70) Cahangirov, S.; Özçelik, V. O.; Rubio, A.; Ciraci, S. *Phys. Rev. B* **2014**, *90* (8), 085426.
(71) He, K.; Poole, C.; Mak, K. F.; Shan, J. *Nano Lett.* **2013**, *13* (6), 2931–2936.
(72) Miró, P.; Ghorbani-Asl, M.; Heine, T. *Angew. Chemie Int. Ed.* **2014**, *53* (11), 3015–3018.
(73) Yu, L.; Zunger, A. *Phys. Rev. Lett.* **2012**, *108* (6), 068701.
(74) Grazianetti, C.; Cinquanta, E.; Tao, L.; De Padova, P.; Quaresima, C.; Ottaviani, C.; Akinwande, D.; Molle, A. *ACS Nano* **2017**, *11* (3), 3376–3382.